An Accurate Large-Signal Model of GaAs MESFET Which Accounts for Charge Conservation, Dispersion, and Self-Heating

Ce-Jun Wei, *Senior Member, IEEE*, Yevgeniy A. Tkachenko, *Member, IEEE*, and Dylan Bartle, *Associate Member, IEEE*

***Abstract*— A comprehensive large-signal model of a GaAs MESFET is presented to account for charge conservation and effects of dispersion and self-heating. An improved set of capacitance and charge equations, along with an enhanced Triquint Own model (TOM)-like drain current model, is used for consistent small- and large-signal simulations. Charge conservation is satisfied by deriving the capacitance part of the model from charge equations. Transconductance and output conductance dispersion is modeled by combination of a feedback network and a subcircuit, which describes the self-heating effect. An improved description of the near-pinchoff characteristics, high-voltage breakdown, and gain compression at high-current region in the TOM is introduced. The new model accurately predicts the *I–V*, CV, bias-dependent S-parameter, waveform, power, and linearity characteristics of the MESFET.**

I. Introduction

GaAs MESFET's exhibit complex nonlinear behavior under large-signal operation and present numerous challenges for accurate device modeling. *I–V* curves of the MESFET show strong dispersion effects causing a discrepancy between the static and dynamic characteristics. A significant difference exists between the dynamic *I–V* characteristics which fit transconductance G_m and those which fit output conductance $G_{\rm ds}$. In addition, charge conservation has to be satisfied for consistent extraction of large- and small-signal models [1], [2]. The charge expressions (QV), which adequately describe capacitance behavior as a function of port voltages (CV), are difficult to obtain. In particular, there is a crossover in measured $C_{\rm gd}$ versus $V_{\rm ds}$ characteristics with varying $V_{\rm gs}$. This crossover was previously overlooked [3]–[5], except for the Chalmers model [6], in which the capacitance curves are fitted with the CV, but not the QV equations.

In this paper, we introduce a model which accounts for the dispersion effects, including self-heating, and accurately fits the measured CV characteristics. It includes a low-pass subthermal circuit to account for the effects of self-heating and a feedback circuit to account for an increased $G_{\rm ds}$ at high frequency. The model satisfies charge conservation and predicts the $C_{\rm gd}(V_{\rm ds})$ crossover behavior. The modeling results were verified by dc, S-parameter, power, waveform, and linearity measurements.

Manuscript received October 8, 1997; revised May 20, 1998.

The authors are with Alpha Industries Inc., Woburn MA 01801 USA (e-mail: cwei@alphaind.com).

Publisher Item Identifier S 0018-9480(98)08023-5.

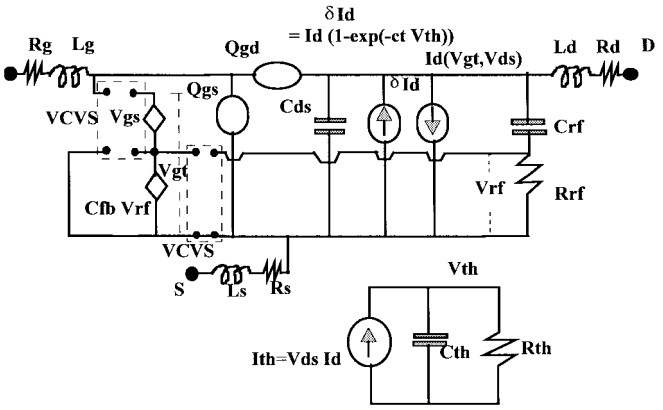

Fig. 1. Equivalent-circuit model of the MESFET to account for self-heating, dispersion, and charge conservation. Gate current is not shown here.

II. Drain Current Model

Triquint's Own model (TOM) [7] was used as a basis for our drain current model. TOM is popular because it can accurately fit the dc behavior of the MESFET. It predicts the negative output conductance at a high dissipated power region, which occurs due to self-heating. However, the negative output conductance is strictly a low-frequency phenomenon ($f <$ 10 MHz) and may cause inaccuracies in high-frequency simulations. Similar to heterojunction bipolar transistors (HBT's) [8], we modeled self-heating with a thermal circuit, which incorporates a normalized unit thermal resistance $(R_{\rm th})$ and a normalized thermal capacitance $(C_{\rm th})$, the product of which is equal to the thermal time constant of the device $T_{\rm th}$ (see Fig. 1). This allows an accurate phenomenological description of self-heating without the knowledge of actual device thermal resistance. The node voltage $V_{\rm th}$ of this circuit represents the normalized rise in temperature, which at dc is equal to the dissipated power in the device. The self-heating causes a decrease in drain current expressed as

$$I_d = I_{d0} \cdot \exp(-C_t \cdot V_{\rm th}) \tag{1}$$

where C_t is the self-heating current-reduction parameter, which is equivalent to the δ parameter in TOM at dc. The

TABLE I
PARAMETERS OF TOM, INCLUDING DISPERSION

Parameter	Description	Unit	Dispersive
β	Transconductance coefficient	A/V	No
V_{t0}	Threshold voltage	V	No
α	Current saturation parameter	1/V	No
γ	Drain–pull parameter	unitless	Yes
δ	Self-heating feedback coefficient	1/W	Yes
Q	Power-law exponent	unitless	No

low-pass nature of this thermal subcircuit results in decreased current reduction with increased frequency. From (1), the reduction of I_d is proportional to the dissipated power $P_{\rm diss}$ when $P_{\rm diss}$ is small, and approaches zero when $P_{\rm diss}$ is extremely large. The dc curves are, therefore, represented as a combination of a TOM description with dc self-heating parameter $\delta = 0$ and a separate self-heating model. With this approach, $G_{\rm ds}$ in the saturation region is positive at high frequencies, as in reality, since the self-heating cannot follow a high-frequency excitation. The measured RF G_m, on the other hand, is reduced with increased dc power dissipation due to increased temperature.

From our experimental results, $G_{\rm ds}$ calculated from the S-parameter measurements is considerably higher than the TOM prediction. To address this discrepancy, we modeled the dispersion of $G_{\rm ds}$ with a high-pass feedback circuit from drain to gate (see Fig. 1), similar to [9]. Unlike the series *RC* representation of dispersion (e.g., EEFET3 or TOM in LIBRA or [10]), this approach allows RF trajectories to reach the pinchoff region without being restricted by the RF resistance. This results in better prediction of power-added efficiency. The effect of this dispersive feedback is translated to setting the parameter γ in TOM to be frequency dependent. The product of $R_{\rm rf}$ and $C_{\rm rf}$, shown in Fig. 1, sets the time constant for $G_{\rm ds}$ dispersion. A small part of RF $V_{\rm ds}$ is fed back to the gate of the MESFET via a voltage-controlled voltage source (VCVS). The gate voltage $V_{\rm gs}$, which appears across $Q_{\rm gs}$, is combined with this feedback voltage by means of another VCVS. The drain current is dependent on the total voltage $V_{\rm gt}$ appearing across both VCVS. In this way, the feedback signal does not directly affect the charge terms. Table I summarizes the TOM parameters and specifies which model parameters are dispersive in our new model. The TOM parameter δ has been replaced with the thermal parameter C_t, and the thermal subcircuit parameter $T_{\rm th}$. The dispersive γ in TOM is replaced by the dc parameter γ, feedback parameter $C_{\rm fb}$, and associated feedback circuit parameters $C_{\rm rf}$ and $R_{\rm rf}$ of the new model.

Most modern power amplifiers for wireless communications are operated under high-impedance loading conditions to achieve high power-added efficiency. In this case, an accurate modeling of the near-pinchoff region is crucial for power performance prediction. In our new model, an additional parameter A is introduced to fit the gradual pinchoff behavior. The new equation is the same as that introduced in [11]

$$I_{\rm ds} = I_d + \ln\{1 + \exp(-A \cdot I_d)\}/A \tag{2}$$

where I_d is expressed in (1) and

$$I_{d0} = \beta \cdot (V_{\rm gs} - V_{t0} + \gamma \cdot V_{\rm ds})Q \cdot \tanh(\alpha \cdot V_{\rm ds}) \cdot {\rm SIGN}(V_{\rm gs} - V_{t0} + \gamma \cdot V_{\rm ds}) \tag{3}$$

where α, β, γ, and Q are the model parameters specified in Table I. Equation (3) is the current in TOM with $\delta = 0$ and $V_{\rm gs} > V_{t0} - \gamma \cdot V_{\rm ds}$. The current in (2) reduces to I_{d0} when $(A \cdot I_{d0}) \gg 1$ and gradually approaches zero when $V_{\rm gs} < V_{t0} - \gamma \cdot V_{\rm ds}$. This allows a more realistic pinchoff behavior compared to most classic models.

Breakdown effects are important for power amplifiers, especially under high-efficiency loading conditions, since the instantaneous drain–gate-voltage swing can reach three times that of the drain bias voltage. Two types of breakdowns exist for MESFET's: pinched- and open-channel breakdowns. The open-channel breakdown is neglected in this paper since, in most power amplifiers, high $V_{\rm ds}$ swing occurs when $V_{\rm gs}$ is near or below the pinchoff region. The pinched-channel breakdown is described by a diode placed between drain and gate with a leakage current I_0 and a large n factor, ranging from 50 to 70, depending on the breakdown voltage. Finally, the gate forward current is modeled in conventional way, as in the Curtice model.

III. CAPACITANCE MODEL

Consistency of large- and small-signal models requires charge conservation condition to be satisfied. Therefore, a small-signal capacitance model (CV) ought to be derived from the charge model (QV). In general, there exist four partial derivatives of the two charge terms, $Q_{\rm gs}$ and $Q_{\rm gd}$ with regard to $V_{\rm gs}$ and $V_{\rm gd}$, respectively, [see Fig. 2(a)]. However, there are only two capacitance elements present in the small-signal equivalent circuit, namely, $C_{\rm gs}$ and $C_{\rm gd}$. These four charge derivatives can be grouped as follows:

$$C_{\rm gd} = \partial(Q_{\rm gs} + Q_{\rm gd})/\partial V_{\rm gd} \tag{4}$$

$$C_{\rm gs} = \partial(Q_{\rm gs} + Q_{\rm gd})/\partial V_{\rm gs}. \tag{5}$$

It can be shown that, for equivalence between the charge and capacitance representations, an additional transcapacitance term $(C_m \cdot V_{\rm gs})$ must be added, as shown in Fig. 2(b). The derivation of equivalency between Fig. 2(a) and (b) is straightforward by comparing the Y-parameters of both circuits. For the forward parameter computation, port 2 is a short, hence, $\delta V_{\rm gd} = \delta V_{\rm gs}$ and one obtains

$$\begin{aligned} Y_{11} &= j\omega(\partial(Q_{\rm gs} + Q_{\rm gd})/\partial V_{\rm gd} + \partial(Q_{\rm gs} + Q_{\rm gd})/\partial V_{\rm gs} \\ &= j\omega(C_{\rm gs} + C_{\rm gd}) \end{aligned} \tag{6}$$

$$\begin{aligned} Y_{21} &= -j\omega(\partial Q_{\rm gd}/\partial V_{\rm gs} + \partial Q_{\rm gd}/\partial V_{\rm gd}) \\ &= -j\omega(C_{\rm gd} - C_m). \end{aligned} \tag{7}$$

For the reverse parameter computation, port 1 is a short, hence, $\delta V_{\rm gd} = -\delta V_{\rm ds}$ and $\delta V_{\rm gs} = 0$ and one obtains

$$Y_{12} = -j\omega\partial(Q_{\rm gs} + Q_{\rm gd})/\partial V_{\rm gd} = -j\omega C_{\rm gd} \tag{8}$$

$$Y_{22} = j\omega\partial(Q_{\rm gs} + Q_{\rm gd})/\partial V_{\rm gd} = j\omega C_{\rm gd}. \tag{9}$$

TABLE II
OVERVIEW OF THE EQUATIONS USED IN THE MODELING

Characteristics	Equations	Remark
Drain-IV	$I_{ds} = I_d + ln\{1 + exp(-A_a \cdot I_d)\}/A_a$ $I_d = I_{do} \cdot exp(-C_t \cdot V_{th})$ $I_{do} = \beta \cdot (V_{gt} - V_{to} + \gamma \cdot V_{ds})^Q \cdot tanh(\alpha \cdot V_{ds}) \cdot SIGN(V_{gs} - V_{to} + \gamma \cdot V_{ds})$ $V_{gt} = V_{gs} + C_{fb} V_{rf}$	Tail near pinch-off Self-heating effect Expression(2),(1), (3) in the text See figue 1
Gate-IV	$Igs=Igo(exp(Vgs/nkT)-1)$ $Igd=Igdo(exp(Vgd/nKT)-1)$	
Breakdown	$I_{bdg}= Ibo(exp(Vdg/n_b)-1)$	High nb value
Gate-source charge	$Q_{gs} = f(V_{gs}, V_{gd}) + C_{gso} \cdot V_{gs}$	expression (13) through (16) in the text
Gate-Drain charge	$Q_{gd} = f(V_{gd}, V_{gs}) + C_{gdo} \cdot V_{gd}$ $f(V_a,V_b) = C_o \cdot \{V_a + C_f \cdot \log(\cosh(S_g \cdot W)/ S_g\}$ $W = V_a - \eta \cdot V_a \cdot V_b - D_c \cdot \tanh(D_k \cdot V_b)$	

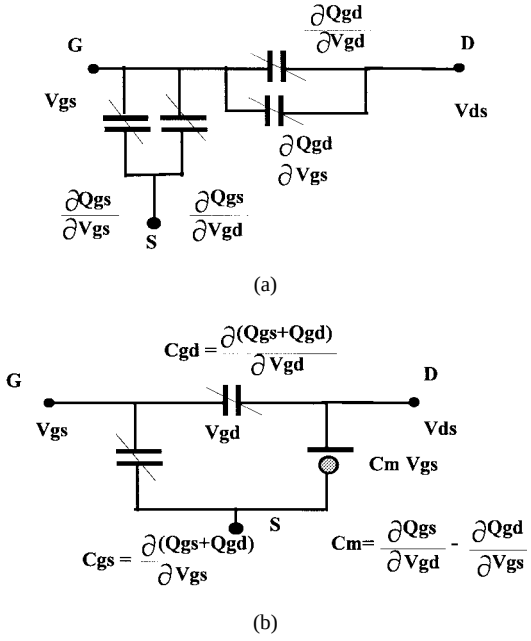

Fig. 2. (a) Capacitance equivalent circuit of the MESFET consistent with charge conservation, which consists of the charge elements. (b) An equivalent of (a), which consists of capacitance elements.

The left equations in (6)–(9) are derived from Fig. 2(a), while the right equations represent conversions from Figs. 2(a) to (b). Full equivalency between the two capacitance representations of the MESFET is achieved by defining a transcapacitance C_m as follows:

$$C_m = \partial Q_{\rm gs}/\partial V_{\rm gd} - \partial Q_{\rm gd}/\partial V_{\rm gs}. \tag{10}$$

This transcapacitance can be translated to a delay time τ by combining it with G_m as follows:

$$G_m = G_{m0} + j\omega C_m = G_{m0}\exp(-j\omega\tau) \tag{11}$$

$$\tau = -C_m/G_{m0}. \tag{12}$$

In this way, conventional small-signal circuits can still be used to satisfy the consistency condition with a large-signal model if the two charge terms are appropriately chosen and the delay time τ is adjusted. Fig. 2 shows the nonlinear capacitance equivalent circuit consistent with the charge conservation condition. To account for the crossover in $C_{\rm gd}(V_{\rm gd}, V_{\rm gs})$, a modification of the Vitesse capacitance model [12] is made by introducing a cross-product term $(V_{\rm gs}) \cdot (V_{\rm gd})$ as follows:

$$Q_{\rm gs} = f(V_{\rm gs}, V_{\rm gd}) + C_{\rm gs0} \cdot V_{\rm gs} \tag{13}$$

$$Q_{\rm gd} = f(V_{\rm gd}, V_{\rm gs}) + C_{\rm gd0} \cdot V_{\rm gd} \tag{14}$$

where

$$f(V_a, V_b) = C_0 \cdot \{V_a + C_f \cdot \log(\cosh(S_g \cdot W)/Sg\} \tag{15}$$

$$W = V_a - \eta \cdot V_a \cdot V_b - D_c \cdot \tanh(D_k \cdot V_b) \tag{16}$$

and $C_{\rm gs0}$, $C_{\rm gd0}$, C_0, C_f, S_g, D_c, η, and D_k are model parameters. All the model equations are summarized in Table II.

IV. PARAMETER-EXTRACTION PROCEDURE

Model extraction was performed using Optotek's LASIMO software,[1] which allows incorporation of user-defined equations for the CV and GV dependencies, element value extraction, and optimization for multiple bias conditions. Since the individual fitting target can include the QV or *I–V* expressions, path independence is not required, and separate sets of equations for $G_{\rm ds}$ and G_m can be independently defined.

The extraction procedure is as follows.

1) Extract parasitic resistance and inductance element values using the cold-FET model [13].
2) Extract 11-element small-signal equivalent-circuit parameters at multiple biases from measured S-parameters.

[1] *LASIMO User's Manual*, OPTOTEK Ltd., Kanata, Ont., Canada K2K 2A9.

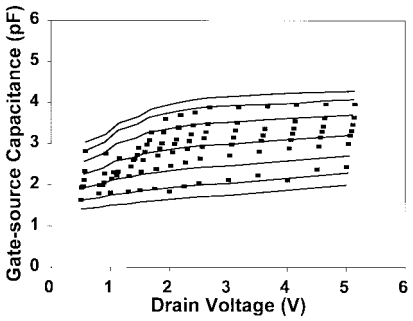

Fig. 3. Measured (symbols) and modeled (lines) gate–source capacitance of a 2-mm MESFET versus $V_{\rm ds}$. $V_{\rm gs} = 0.6, \cdots, -1.8$ V top down.

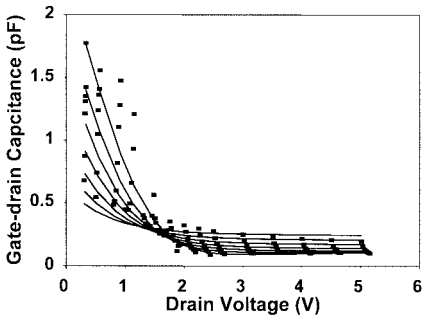

Fig. 4. Measured (symbols) and modeled (lines) gate-drain capacitance of a 2-mm MESFET versus $V_{\rm ds}$. $V_{\rm gs} = 0.6, \cdots, -1.8$ V top down.

3) Extract nonlinear capacitance model parameters by fitting $C_{\rm gs}$ and $C_{\rm gd}$ only. The transcapacitance C_m or delay time τ are used for verification of charge conservation.
4) Extract TOM parameters with $\delta = 0$ and self-heating parameters by fitting $G_{\rm ds}$ and G_m, where

$$G_m = \exp(-C_t \cdot V_{\rm th}) \cdot \partial I_{\rm ds}/\partial V_{\rm gs} \tag{17}$$

$$G_{\rm ds} = \exp(-C_t \cdot V_{\rm th}) \cdot \partial I_{\rm ds}/\partial V_{\rm ds}. \tag{18}$$

TOM parameter γ is optimized to yield $\gamma_{\rm RF}$, which includes the contribution of RF feedback to fitting of $G_{\rm ds}$. Note that due to a large thermal time constant, the self-heating effect or the $V_{\rm th}$, which is equal to power dissipation in measurement, is affected only by the bias point, and results in the decrease of both measured G_m and $G_{\rm ds}$ with increased power dissipation, but $G_{\rm ds}$ always remains positive.
5) Fit the dc characteristics by keeping all parameters unchanged and enabling only γ to vary. The difference between the newly obtained γ and $\gamma_{\rm RF}$ is the feedback parameter $C_{\rm fb}$.

The model was developed for a standard 0.7-μm gate Alpha Industries' MESFET. Approximately 400 dc and S-parameter measurements were taken at different biases, including ten bias points for cold-FET ($V_{\rm ds} = 0$ V) extraction. The bias ranges included from -2 to 0.6 V for $V_{\rm gs}$ and from 0 to 5 V for $V_{\rm ds}$.

The modeling results were compared for the Statz, modified Statz, Vitesse, and our new model. In the modified Statz model, parameters in the CV expressions can be tuned independently of those in the *I–V* expressions. On the contrary, the conventional Statz CV model in conjunction with the TOM *I–V*

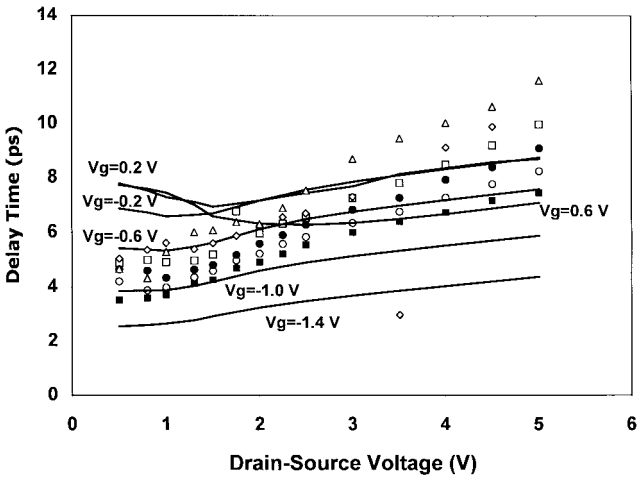

Fig. 5. Modeled (lines) versus measured (symbols) delay time as a function of $V_{\rm ds}$, $V_{\rm gs}$ of a 2-mm MESFET.

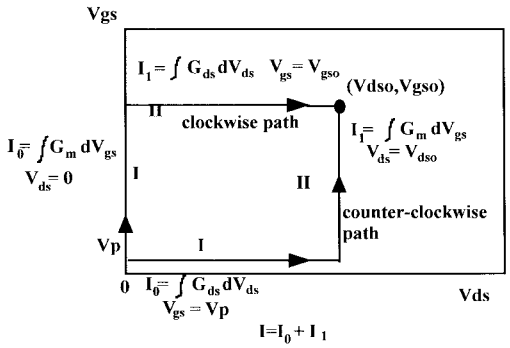

Fig. 6. Illustration of clockwise and counterclockwise integration paths in the $V_{\rm gs}$–$V_{\rm ds}$ plane for current calculation.

model has several parameters shared by the *I–V* and CV characteristics. After optimization, the errors in fitting the CV characteristics were 16.7%, 8.9%, 9.5%, and 5.8% for the Statz, modified Statz, Vitesse, and the new model, respectively, indicating a better fitting for our new model. Figs. 3 and 4 show the fitting results for $C_{\rm gs}$ and $C_{\rm gd}$ as a function of $V_{\rm ds}$ with varying $V_{\rm gs}$. Clearly, the crossover in $C_{\rm gd}$ behavior is predicted well. Fig. 5 plots the modeled delay time (lines) based on (10) and (12) with the measured (symbols). Note that the charge parameters are extracted by fitting $C_{\rm gs}$ and $C_{\rm gd}$, but not C_m. Nevertheless, the delay time τ agrees reasonably well with the measured data, as shown in the figure. This relative consistency verifies the charge conservation as formulated by (10) and (12).

The *I–V* model was generated by fitting the RF *I–V* characteristics, which were obtained by integration of the measured Y-parameters at 1 GHz. It is assumed that integration is frequency-independent. Integration of $\mathrm{Re}[Y21] = G_m$ and $\mathrm{Re}[Y22] = G_{\rm ds}$ for calculation of I_d was performed via the clockwise and counterclockwise paths on the $V_{\rm gs}$–$V_{\rm ds}$ plane indicated in Fig. 6. The integration of drain current is composed of two parts: I and II. The first part of integration results in a small contribution to the current, as specified in the figure as I_0, and the major contribution comes from the second part of integration, represented by I_1, where $G_{\rm ds}$ and G_m

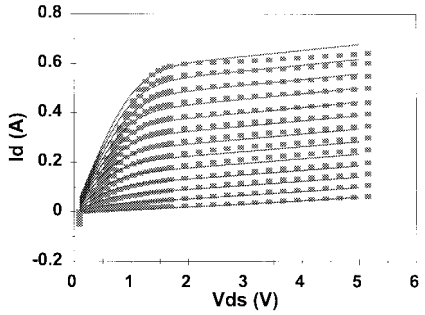

Fig. 7. Comparison between modeled output RF *I–V* characteristics of a 2-mm MESFET obtained by fitting G_m (lines) and *I–V* characteristics obtained by counterclockwise integration in the $V_{\rm gs}$–$V_{\rm ds}$ plane (symbols). $V_{\rm gs} = 0.6, \cdots, -1.8$ V top down.

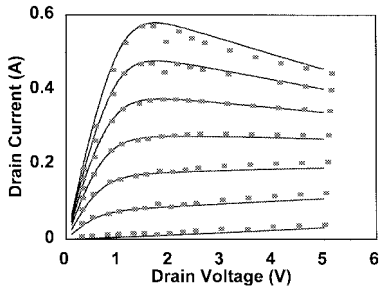

Fig. 8. Comparison between modeled (lines) and measured (symbols) output dc *I–V* characteristics of a 2-mm MESFET. $V_{\rm gs} = 0.6, \cdots, -1.8$ V top down.

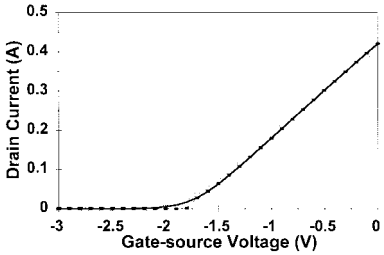

Fig. 9. Comparison between the measured characteristics (points), and those predicted by the new model (line) of the dc transfer characteristics of a 2-mm MESFET at $V_{\rm ds} = 2$ V. The dotted line near pinchoff was the simulated results with the TOM model.

play the dominate role in the clockwise and counterclockwise paths, respectively. Therefore, the data obtained by counterclockwise integration were fitted by optimizing G_m with other parameters being relaxed, whereas in the case of clockwise integration, $G_{\rm ds}$ is optimized. The resulted counterclockwise RF curves are found very close to the dc characteristics. The clockwise RF *I–V* curves, as shown in Fig. 7, show positive slopes, indicating that the negative resistance in the higher current region is purely a low-frequency phenomenon. Fitting of the dc *I–V* characteristics was accomplished by setting $C_{\rm fb} = 0$. The measured and modeled dc output characteristics are shown in Fig. 8. To minimize the overall fitting error of the dc and two sets of RF *I–V* characteristics, model parameters other than γ and $C_{\rm fb}$ are adjusted.

Fig. 9 shows that the new model accurately describes the near-pinchoff region of the measured transfer characteristics at $V_{\rm ds} = 2$ V. The fitting is improved compared to the conventional TOM description, which predicts abrupt pinchoff.

TABLE III
PARAMETERS OF THE NEW MODEL AND THEIR EXTRACTED VALUES

	Parameter	Value	Unit
Drain current coefficients	β	0.216	A/V
	V_{to}	-1.813	V
	γ	0.450	unit-less
	Q	1.261	unit-less
	C_t	0.133	1/W
	T_{th}	0.100	μs
	C_{fb}	0.049	unit-less
	Aa	85	1/A
Capacitance parameters	C_0	1.58	pF
	S_g	0.89	1/V
	η	-0.025	V-2
	D_c	0.42	V
	D_k	0.63	V
	C_{gs0}	0.71	pF
	C_{gd0}	0.06	pF
	C_f	0.96	V
	$V1$	1.5	V
Extrinsic parasitic parameters	R_s	0.35	Ω
	R_d	0.46	Ω
	R_g	1.75	Ω
	L_s	7.7	pH
	L_d	62.4	pH
	L_g	54.6	pH

Table III summarizes the extracted model parameter values for the 2-mm MESFET.

V. MODEL VERIFICATION

The new model was implemented as a user-defined element in LIBRA. Small- and large-signal characteristics of the 2-mm MESFET were simulated and measured in the 50-Ω system. The thermal time constant was set to 50 μs, while the dispersion time constant was set to 1 μs ($C_f = 10^{-14}$ F, $R_f = 10^8$ Ω) for continuous wave (CW) simulations. For comparison, the TOM *I–V* model in conjunction with the Statz CV model was extracted and implemented in LIBRA.

Fig. 10 shows the comparison between the measured and simulated S_{11}, S_{22}, and S_{21} based on the large-signal model at $V_{\rm ds} = 4$ V and $V_{\rm gs} = -1.6$ V. The modeled results with dispersive TOM model are also shown. The conventional TOM model does not take into account the difference between the dc $G_{\rm ds}$ and RF $G_{\rm ds}$ and, hence, gives erroneous results, which significantly deviate from measurements. Therefore, a built-in LIBRA dispersive TOM model was then used for a comparison. The dispersive TOM model is generated by fitting the dc *I–V*'s, RF $G_{\rm ds}$ and the CV's and assuming that dispersion parameters $R_{\rm db} = 10$ MΩ and $C_{\rm db} = 1$ fF. Fig. 11 shows that for the new model, the modeled and measured S-parameters are in good agreement for both the lower current bias of $V_{\rm ds} = 4$ V and $V_{\rm gs} = -1.6$ V and higher current bias of $V_{\rm ds} = 4$ V and $V_{\rm gs} = 0.2$ V. For the dispersive TOM model, much higher $|S_{21}|$ and $|S_{22}| > 1.0$ for higher current bias were obtained. This happened because in order

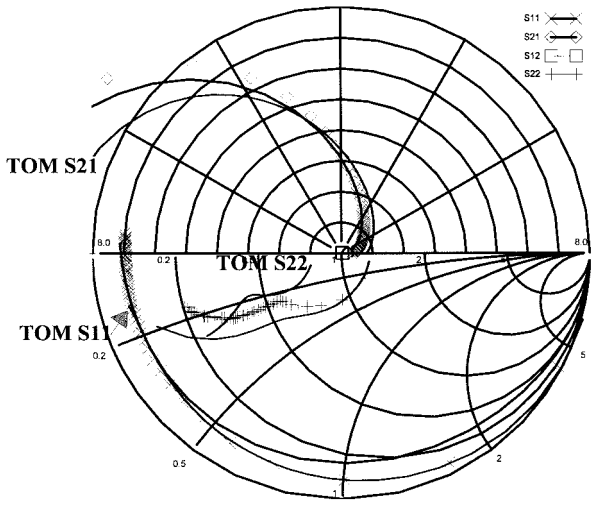

Fig. 10. Measured (symbols) and modeled (lines) S-parameters of a 2-mm MESFET at $V_{\rm ds} = 4$ V, $V_{\rm gs} = -1.6$ V. Results for the TOM model are also shown for comparison.

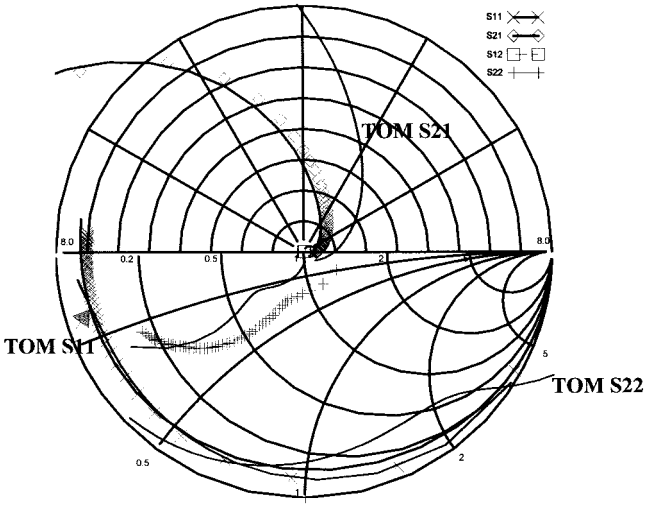

Fig. 11. Measured (symbols) and modeled (lines) S-parameters of a 2-mm MESFET at $V_{\rm ds} = 4$ V, $V_{\rm gs} = 0.2$ V. Results for the TOM model are also shown for comparison.

to fit the dc *I–V* curves and RF $G_{\rm ds}$ at the lower current region, this model always predicts higher output resistance over a wide bias range, and even negative resistance at high current region, resulting in S_{22} of either large magnitude or outside the Smith chart.

Fig. 12 shows the simulated power performance of the device biased at $V_{\rm gs} = -1.7$ V and $V_{\rm ds} = 3$ V. It can be seen that the model predicts well the power gain, output power, and power-added efficiency. The slight discrepancy between the measured and simulated results is attributed to the extrapolation error outside the region where the S-parameters used for extraction were measured. The simulated results using the dispersive TOM model are also plotted in Fig. 12 for comparison. It is seen that the TOM model predicts higher than measured gain, power output and power-added efficiency.

Fig. 13(a) and (b) shows that a good agreement is obtained between the measured and simulated voltage and current

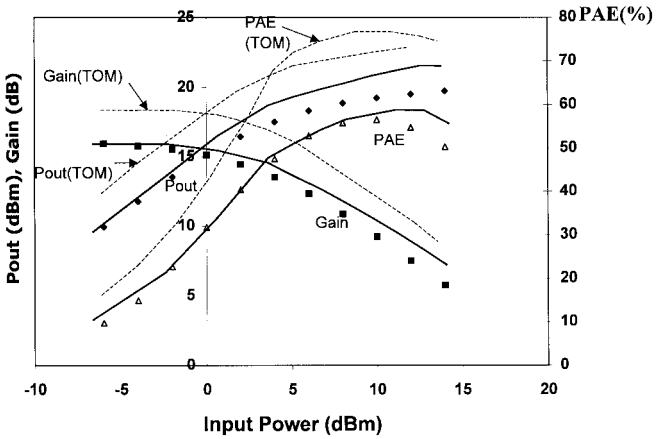

Fig. 12. Measured (solid symbols) and modeled (lines) power, power-added efficiency, and gain performance of a 2-mm MESFET at $V_{\rm ds} = 3$ V, $V_{\rm gs} = -1.7$ V. Results for the TOM model are shown by broken lines. The arrows show the difference between measured characteristics and those modeled with the TOM model at selected input powers.

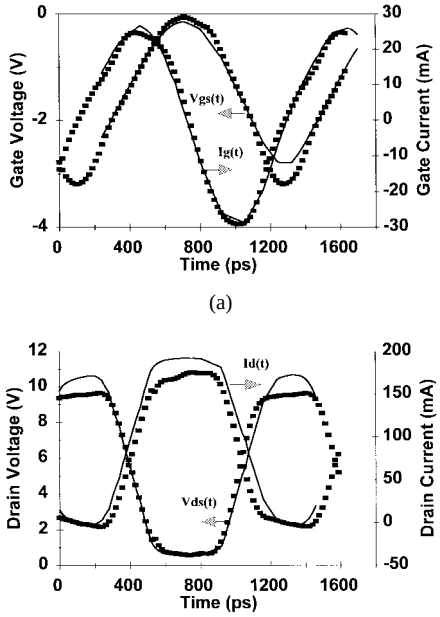

Fig. 13. Measured (symbols) and modeled (lines) (a)$V_{\rm gs}$, I_g and (b) $V_{\rm ds}$, I_d waveforms of a 2-mm MESFET at $V_{\rm ds} = 5$ V, $V_{\rm gs} = -1.4$ V, and $P_{\rm in} = 10$ dBm.

waveforms of the MESFET at $V_{\rm ds} = 4$ V and $V_{\rm gs} = -1.4$ V and input drive level of 10 dBm. The waveforms were measured in the 50-Ω system at 0.85 GHz by using a microwave-transition-analyzer-based system reported in [14]. It can be seen that the model predicts clamping of both the drain voltage and drain current waveforms by the pinchoff and linear regions of the output *I–V* characteristics. The output waveforms, therefore, contain higher harmonics, whereas the input waveforms contain some degree of the second harmonic only. Waveform analysis serves as a direct verification of the model.

MESFET intermodulation distortion was simulated under two-tone excitation conditions at $V_{\rm ds} = 5$ V and $V_{\rm gs} = -1.4$ V. Tones were separated by 10 kHz and f_1 was 0.85 GHz. For

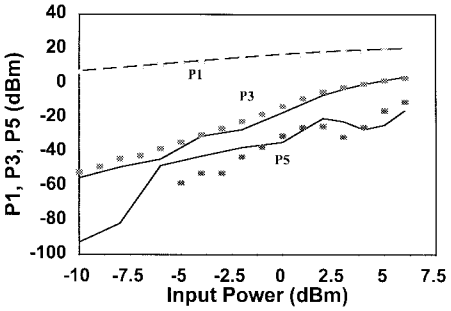

Fig. 14. Measured (symbols) and modeled (lines) single-tone power ($P1$), third intermodulation ($P3$), and fifth intermodulation ($P5$) of a 2-mm MESFET versus input power per tone. $V_{\rm ds} = 5$ V, $V_{\rm gs} = -1.4$ V.

simplicity, 50-Ω matching was chosen on both input and output. Fig. 14 shows that the simulated single-tone output power and the third- and fifth-order intermodulation products versus input power per tone are in agreement with the measured data.

VI. Conclusion

A new comprehensive and robust model for GaAs MESFET's was presented. The model takes into account dispersion and self-heating effects and satisfies charge conservation criterion. This results in consistency between the large- and the small-signal models. The model parameters associated with CV, *I–V* and dispersion were extracted without extensive cross-tuning. The verification of the new model includes dc *I–V*, CV, bias-dependent S-parameter, CW power, two-tone linearity, and waveform analysis.

References

[1] P. Jansen, D. Schreurs, W. De Raedt, B. Nauwelaers, and M. Van Rossum, "Consistent small-signal and large-signal extraction techniques for heterojunction FET's," *IEEE Trans. Microwave Theory Tech.*, vol. 43, pp. 87–93, Jan. 1995.

[2] C. J. Wei, J. W. Bao, and J. C. M. Hwang, "Novel experimentally based modeling for MESFET's having complex dispersion effects," in *IEEE on Workshop Experimentally Based FET Modeling Related Nonlinear Circuit Design*, Kassel, Germany, 1997, pp. 22.1–22.8.

[3] H. Statz, P. Newman, I. Smith, R. Pucel, and H. Haus, "GaAs FET device and circuit simulation in SPICE," *IEEE Trans. Electron Devices*, vol. ED-34, pp. 160–169, Feb. 1987.

[4] N. Scheinberg and E. Chisholm, "A capacitance model for GaAs MESFET's," *IEEE J. Solid-State Circuits*, vol. 26, pp. 1467–1470, Oct. 1991.

[5] M. Berroth, "Circuit simulation for hetero-structure field-effect transistors," Ph.D. dissertation, Dept. Elect. Eng., Univ. Bochum, Bochum, Germany, 1991.

[6] I. Angelov, H. Zirath, and N. Rorsman, "A new empirical nonlinear model for HEMT and MESFET devices," *IEEE Trans. Microwave Theory Tech.*, vol. 40, pp. 2258–2266, Dec. 1992.

[7] A. McCamant, G. McCormack, and D. Smith, "An improved GaAs MESFET model for SPICE," *IEEE Trans. Microwave Theory Tech.*, vol. 38, pp. 822–824, June 1990.

[8] C. J. Wei, W. J. Ho, and J. C. M. Hwang, "Large-signal modeling of self-heating, collector transit-time, and RF-breakdown effects in power HBT's," *IEEE Trans. Microwave Theory Tech.*, vol. 44, pp. 2641–2647, Dec. 1996.

[9] K. Jeon, Y. Kwon, and S. Hong, "A frequency dispersion model of GaAs MESFET for large-signal applications," *IEEE Microwave Guided Wave Lett.*, vol. 7, pp. 78–80, Mar. 1997.

[10] R. Follman, R. Tempel, T. Sporkmann, and I. Wolff, "A new spline-based FET model for MESFET's and HEMT's," in *27th European Microwave Symp. Dig.*, Jerusalem, Israel, Sept. 1997, pp. 1360–1366.

[11] C. J. Wei, Y. Lan, Y. A. Tkachenko, and J. C. M. Hwang, "A nonlinear high-frequency MESFET amplifier model verified by waveform and load-pull measurements," in *43rd ARFTG Conf. Dig.*, San Diego, CA, May 1994, pp. 117–120.

[12] J. Kotz, "An improved capacitance model for GaAs MESFET's," in *GaAs IC Symp. Dig.*, Orlando, FL, Nov. 1996, pp. 171–174.

[13] G. Dambrine, A. Cappy, F. Heliodore, and E. Playez, "A new method for determining the FET small-signal equivalent circuit," *IEEE Trans. Microwave Theory Tech.*, vol. 36, pp. 1151–1159, July 1988.

[14] C. J. Wei, Y. A. Tkachenko, and J. C. M. Hwang, "Non-invasive waveform probing for nonlinear network analysis," *Microwave J.*, pp. 122–126, Feb. 1994.

Ce-Jun Wei (M'92–SM'98) graduated from Tsing-Hua University, Beijing, China, in 1962. He received the Ph.D. degree from Academica Sinica, Beijing, China, in 1983.

From 1966 to 1980, he was with the Chinese Academy of Sciences. From 1982 to 1986, he was a Research Professor, responsible for development of microwave devices and circuits. From 1980 to 1982, he was with Aachen Technical University. From 1986 to 1988, he was a Visiting Professor at Herz-Heinrich Institute and Berlin Technical University, respectively, working in the area of opto-electronics. From 1989 to 1996, he was a Senior Scientist at Lehigh University. In 1997, he joined Alpha Industries Inc., Woburn, MA, where he is currently a Principal Engineer. He has authored and co-authored over 60 papers. His current interest is in microwave device modeling and characterization technique.

Dr. Wei was the recipient of the Alexander Von Humboldt Foundation Fellowship (1980–1982).

Yevgeniy A. Tkachenko (S'92–M'95) graduated from Kiev Polytechnical Institute, Kiev, Ukraine, and received the B.S., M.S. and Ph.D. in electrical engineering from Lehigh University, Bethlehem, PA, in 1991, 1993 and 1995, respectively.

He is currently an Engineering Manager at Alpha Industries, Inc., Woburn, MA. He has authored and co-authored 25 technical papers. His interests include GaAs MESFET and pHEMT device development, characterization, modeling and reliability.

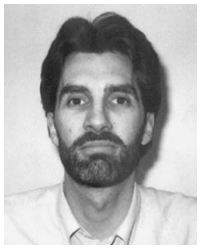

Dylan Bartle (A'93) received the B.S. degree with honours in chemical physics from the University of Reading, Reading, U.K., in 1981. He also received a post-graduate diploma in electronic and molecular properties of materials from Thames Polytechnic London, London, U.K.

From 1981 to 1986, he worked in the compound semiconductor division, GEC Research Laboratories, London, U.K., where he was responsible for development of ion-implanted GaAs MESFET's and diode devices for microwave monolithic microwave integrated circuits (MMIC's). In 1986, he joined Alpha Industries, Inc., Woburn, MA, where he works on many product and process development projects for discrete GaAs devices and MMIC's, including MESFET, high electron-mobility transistor (HEMT), and pseudomorphic HEMT (pHEMT) devices for power amplifier, low-noise amplifier, and switch functions for both military and commercial applications from L- to W-bands, monolithic p-i-n diodes for high-power Ka-band switch applications, Schottky diode devices, and some multifunction MMIC's. He is currently Engineering Manager in the GaAs Wafer Laboratory. He has authored and co-authored several papers on GaAs device and process technology.